Palaeogeography, Palaeoclimatology, Palaeoecology 655 (2024) 112507

Contents lists available at ScienceDirect

Palaeogeography, Palaeoclimatology, Palaeoecology

journal homepage: www.elsevier.com/locate/palaeo

Extreme drought events and land surface temperature variations on the northeastern Tibetan Plateau over the last 350 ka

Shaohua Tian [a], Gaowen Dai [a], Guoqiao Xiao [b,*], Huan Yang [b], Xiaoqing Meng [b], Qiuzhen Yin [c]

[a] State Key Laboratory of Biogeology and Environmental Geology, School of Earth Sciences, China University of Geosciences, Wuhan 430074, China
[b] Hubei Key Laboratory of Critical Zone Evolution, School of Geography and Information Engineering, China University of Geosciences, Wuhan 430078, China
[c] Earth and Climate Research Center, Earth and Life Institute, Universite catholique de Louvain, Louvain-la-Neuve 1348, Belgium

ARTICLE INFO

Editor: B Shen

Keywords:
Northeastern Tibetan Plateau
Quaternary
GDGTs
Paleo-temperature
Extreme drought

ABSTRACT

The northeastern Tibetan Plateau (NETP) is located in the ecologically vulnerable northwestern China, with semi-humid and semi-arid conditions. Long-term paleo-hydrological and paleo-temperature variations and their mechanisms over the NETP remain ambiguous, primarily due to the limited availability of well-dated, long-term depositional archives and suitable proxies. In this paper, we investigate climate variations and their underlying mechanisms in the region using Glycerol Dialkyl Glycerol Tetraethers (GDGTs) spanning the last 350 ka. Our results suggest that the NETP underwent substantial drying during glacial periods, with the driest period occurring during the last glacial period. The intensity of drought during glacial periods is comparable to that in the Westerlies-dominated region but differs from that in the East Asian monsoon region. This suggests that the influence of the Westerlies surpassed that of the East Asian summer monsoon (EASM), becoming the major driver of warm-season drought events on the NETP during glacial periods. Additionally, the peaks of aridity events coincide with summer insolation maxima during glacial periods, which may be related to the direct influence of local insolation on regulating evaporation. The reconstructed land surface temperatures were about 6.7 °C during interglacial periods and 2.6 °C during glacial periods, which may be linked to a combination of variations in insolation, CO_2 levels, and other internal feedback mechanisms. However, an unusual warming occurred during the last glaciation, with an average temperature of about 4.8 °C. This warming may be related to variations in soil moisture and vegetation resulting from extreme drought. Our study highlights the sensitivity of hydrological variations over the NETP to insolation and Westerlies, as well as the critical roles of soil moisture and vegetation in land surface temperature variations.

1. Introduction

The NETP (Fig. 1A) is located in ecologically vulnerable northwestern China, where its climate currently oscillates between semi-humid and semi-arid conditions (Liu et al., 2017). Paleoclimate changes in this region are influenced by both the Asian monsoon and the Westerlies (An et al., 2012). Over the last few years, the mean annual air temperature (MAAT) on the Tibetan Plateau has increased at twice the global average rate (Chen et al., 2015), primarily due to its high climate sensitivity. As one of the driving forces behind both regional and global environmental changes (Kang et al., 2010), variations in drought and temperature over the NETP exert a significant influence on the region's ecosystems (Zou et al., 2020), as well as on dust transportation (Xiao et al., 2012, 2023; Stauch et al., 2012; Liu et al., 2017), and temperature and precipitation variations (Wu and Qian, 2003; Ding and Chan, 2005; Hsu and Lin, 2007) in the densely populated Eastern Asian continent.

Over the past few decades, numerous studies have used various proxies to reconstruct paleo-humidity variations in the NETP, particularly since the last glacial period. These studies have found that the NETP experienced an arid climate (Lu et al., 2012; An et al., 2012; Wang et al., 2017), with less vegetation (e.g., Wischnewski et al., 2011; Cheng et al., 2013; Li et al., 2017) and significant desertification (e.g., Stauch et al., 2012; Liu et al., 2017) during the last glacial period. However, this trend reversed in the Holocene (Thomas et al., 2016a; Chen et al., 2016). Despite this, our understanding of paleo-humidity variations in the NETP before the last glacial period remains limited, primarily due to the scarcity of long-term depositional archives caused by intense glacial and wind erosion in the region.

* Corresponding author.
E-mail addresses: gqxiaocug@126.com, xgqiaocug@gmail.com (G. Xiao).

https://doi.org/10.1016/j.palaeo.2024.112507
Received 4 June 2024; Received in revised form 10 September 2024; Accepted 17 September 2024
Available online 19 September 2024

Further, the mechanisms behind paleo-humidity changes over the NETP remain ambiguous. Some scholars posit that the arid climate during the last glacial period and the humid climate in the Holocene over the NETP were controlled by the Westerlies and the EASM, respectively (e.g., An et al., 2012; Thomas et al., 2016a; Sun et al., 2019). Others propose that the high-altitude climate variations of the NETP were controlled by the Westerlies from the last glacial maximum onwards (Fan et al., 2014; Li et al., 2020). A third standpoint attributes the episodic aridification during the last glacial period to the intensification of the Siberian high-pressure cell (Wang et al., 2017; Yang et al., 2017). Additionally, Lu et al. (2004, 2006, 2012) emphasized the importance of the Tibetan Plateau Monsoon.

In contrast to paleo-humidity, there are fewer climate records available for reconstructing paleo-temperature variations across the NETP. These studies mainly focus on the last deglaciation and the Holocene (e.g., Herzschuh et al., 2009, 2010; Hou et al., 2016; Sun et al., 2019; Duan et al., 2019; Wang et al., 2021), with particular emphasis on the Holocene. They have demonstrated that the temperature fluctuations during the Holocene were related to insolation, CO_2 levels, and internal feedbacks associated with precipitation and vegetation (Liu et al., 2009; Zhang et al., 2014; Wang et al., 2021). However, our knowledge of variations in paleo-temperature and their underlying mechanisms before the last glacial period in this region is limited, primarily due to the absence of suitable paleo-temperature proxies and continuous long-term archives (Herzschuh et al., 2006, 2009; Zhu et al., 2008; Zhao et al., 2020).

GDGTs, derived from the membranes of certain archaea and bacteria, occur ubiquitously in various environments (e.g., Peterse et al., 2011; Schouten et al., 2013; Zhu et al., 2024) and are highly sensitive to changes in temperature and humidity (Weijers et al., 2007; Peterse et al., 2012; De Jonge et al., 2014). The ratio of archaeal isoprenoid GDGTs (isoGDGTs) to bacterial branched GDGTs (brGDGTs), denoted as $R_{i/b}$, shows a sharp increase when soil pH > 7.5 and mean annual precipitation < 600 mm (Xie et al., 2013), and exhibits a significant correlation with soil water content in the surface soil from the NETP (Dang et al., 2016). Hence, $R_{i/b}$ has been proposed as an indicator of extreme drought events in terrestrial settings (Xie et al., 2013; Yang et al., 2014). The 6-methyl brGDGTs, e.g., IIa', are closely related to soil pH, while 5-methyl brGDGTs, e.g., Ia, exhibit less correlation with soil pH (De Jonge et al., 2014). Thus, the $IR_{IIa'}$ ratio can be used as paleo-pH indicator (De Jonge et al., 2014; Yang et al., 2015). The ratio of GDGT-0 to Crenarchaeol (GDGT-0/Cren) is closely related to dissolved oxygen in the water column and precipitation (Qian et al., 2019) and has the potential to reconstruct paleo-hydroclimate changes (Lu et al., 2021).

Simultaneously, various GDGT-derived paleo-temperature proxies (e.g., MBT'_{5ME}, $MBT_{5/6}$, MAATmr, Index 1, Index 2) have been developed and frequently employed to reconstruct temperature variations in loess-paleosol sequences on the Chinese Loess Plateau (e.g., Peterse et al., 2011, 2014; Gao et al., 2012; Jia et al., 2013; Thomas et al., 2016b; Lu et al., 2016, 2019; Tang et al., 2017a, 2017b; Zhao et al., 2018; Zeng and Yang, 2019; Guo et al., 2024) and the NETP (e.g., Duan et al., 2019; Sun et al., 2019; Wang et al., 2021).

Recently, we investigated a high-resolution loess section spanning the past 420 ka from the Menyuan Basin on the NETP (Fig. 1B). The section exhibits strong signals of ~20-kyr climate cycles (Tian et al., 2022; Xiao et al., 2023) and thus serves as an ideal archive for studying long-term paleoclimate changes on the NETP. The objectives of this study are: (1) to reconstruct extreme drought events and hydrological variations on the NETP by utilizing the $R_{i/b}$, $IR_{IIa'}$, and GDGT-0/Cren proxies, and to investigate their forcing mechanisms; and (2) to quantitatively reconstruct the land surface temperature changes on the NETP based on GDGT temperature proxies and explore potential causal mechanisms. Our study provides the first paleo-temperature record spanning such a long timescale over the NETP.

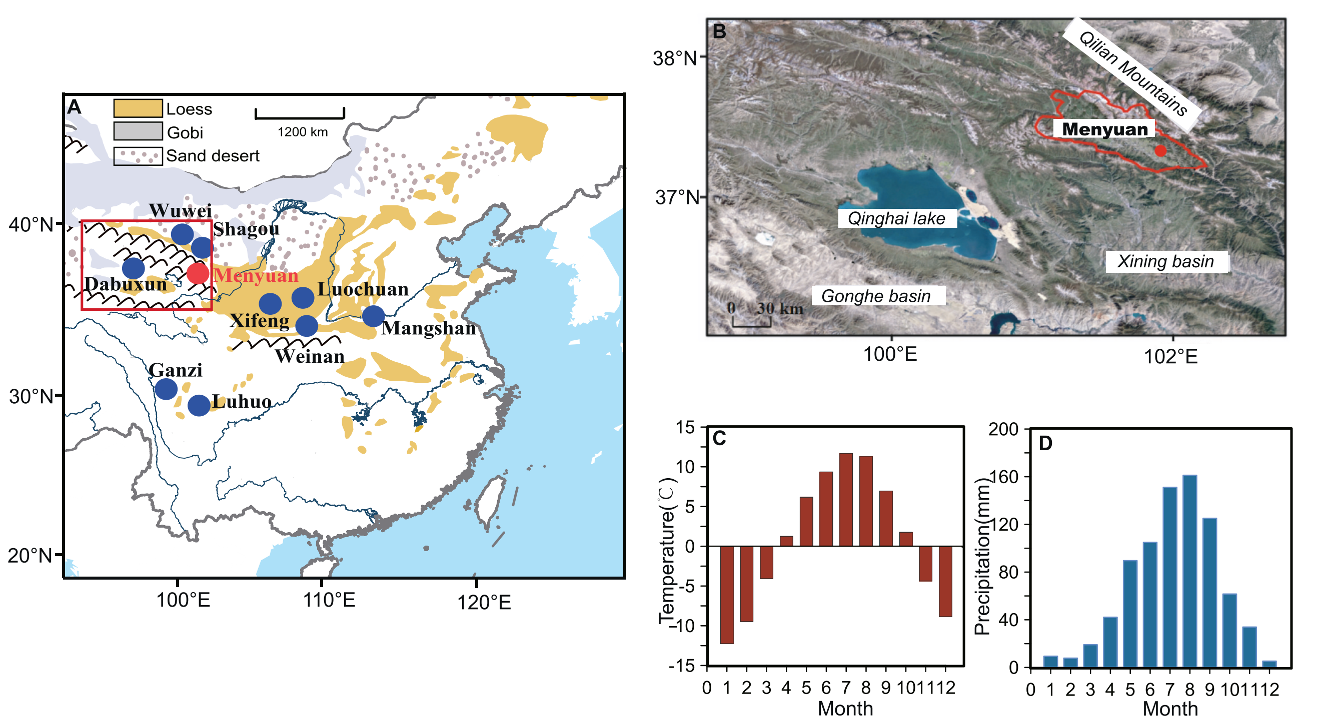

Fig. 1. (A) Location of the NETP and sites mentioned in the text; (B) Location of the Menyuan Basin and the Menyuan loess section; (C) Modern monthly mean temperature and (D) monthly mean precipitation for the Menyuan Basin.

2. Materials and methods

2.1. General settings

The Menyuan Basin is located in the eastern part of the Qilian Mountains at an average altitude of approximately 2800 m. It is bordered by the Daban Mountains to the south and the Lenglongling Mountains to the north. The Datong River flows through the Menyuan Basin from the northwest to the southeast. Currently, the Asian summer monsoon affects this region during the summer, while the Westerlies dominate the winter climate, primarily because the high mountains along the northern edge of the basin block the East Asian winter monsoon (An et al., 2012). The modern monthly mean annual temperature in the region is 0.8 °C, ranging from −12 °C in January to 12 °C in July (Fig. 1C). From May to September, temperatures vary between 6.2 °C and 12 °C (Fig. 1C). The monthly mean annual precipitation is 520 mm, with a significant difference between winter and summer. The maximum precipitation occurs in August at 161.2 mm, while the minimum is in December at 10 mm (based on China Meteorological Administration climate records during 1981–2010, http://www.cma.gov.cn).

2.2. Studied section and methods

The Menyuan loess section (37.33°N, 101.82°E, 2838 m above sea level) is located on the fifth terrace (T5) of the Datong River. It comprises five paleosol layers (S0–S4) and four loess units (L1–L4). The Holocene paleosol S0 is silty black loam with a thickness of ~2 m. The S1 (10 m thick) and S2 (6 m thick) units are black loam with more pronounced pedogenesis compared to S0. Menyuan loess grain size and magnetic susceptibility curves correspond well with those of the Gulang loess section (Fig. S1). For example, the grain size curve of S1 in the Menyuan section exhibits three peaks at 23.5, 27.9 and 29.7 m, which correspond well to the three peaks of S1 in the Gulang section (Fig. S1). Ultimately, 19 tie points were adopted to refine the chronology of the Menyuan section by correlating our grain size and magnetic susceptibility curves with those of the Gulang section. Our results reveal that the basal age of the Menyuan section is ~420 ka (Fig. S1; Tian et al., 2022), aligning with the electron spin resonance dating results from the fluvial conglomerates of terrace T5 (Ma et al., 2020).

We only measured the samples from the section after 350 ka because the lower part of the section was likely contaminated to some extent by the Paleogene red bed materials. GDGT records have a resolution of approximately 3500 years. All the GDGTs samples were dried in an oven at 40 °C, then ground to a powder. Samples were extracted with a mixture of dichloromethane (DCM): methanol (9:1, v: v) using an Accelerated Solvent Extractor (ASE 100, Dionex). The total extracts were concentrated and then separated into non-polar and polar fractions on silica gel column by using *n*-hexane and methanol, respectively. The polar fraction was filtered through a 0.45 μm PTFE syringe filter and then was dissolved again in *n*-hexane/isopropanol, with standard C_{46} GTGT added. GDGTs were determined using an Agilent 6460 A triple quadrupole mass spectrometer (LC-MS/MS). The elution gradient follows Yang et al. (2015). Detection was achieved in an atmospheric pressure chemical ionization chamber with selected ion monitoring at *m/z* 1302, 1300, 1298, 1296, 1292, 1050, 1048, 1046, 1036, 1034, 1032, 1022, 1020, 1018, and 744.

Various GDGT-derived proxies were employed for this study to reconstruct paleo-temperature and paleo-hydrological variations. The temperature, pH, GDGT-0/Cren, and $R_{i/b}$ were calculated using the calibration equations provided in Tables 1 and 2. Roman numerals in tables correspond to the molecular structures of GDGTs.

Table 1
Definitions for GDGT indices. MBT′: Methylation index of Branched Tetraethers. MBT'_{5ME}: Exclusion of the 6-methyl brGDGTs from the MBT′.

Index	Definition	Reference
$R_{i/b}$	$R_{i/b} = (\sum isoGDGTs)/(\sum brGDGTs)$	Xie et al., 2013
$IR_{IIa'}$	$IR_{IIa'}$ = IIa'/ (IIa + IIa')	De Jonge et al., 2014
GDGT-0/Cren	GDGT-0/Cren	Qian et al., 2019
MBT'_{5ME}	MBT'_{5ME} = (Ia + Ib + Ic)/(Ia + IIa + IIIa+Ib + IIb + Ic + IIc)	De Jonge et al., 2014
$MBT_{5/6}$	$MBT_{5/6}$ = (Ia + Ib + Ic + IIa')/ (Ia + Ib + Ic + IIa + IIb + IIc + IIIa + IIIa')	Ding et al., 2015
Index 1	Index 1 = log [(Ia + Ib + Ic + IIa' + IIIa')/ (Ic + IIa + IIc + IIIa + IIIa')]	De Jonge et al., 2014

Table 2
Calibrations for pH and temperature proxies. MAAT: Mean Annual Air Temperature. MAST: Mean Annual Soil Temperature. RMSE: Root Mean Squared Error.

Calibration	Reference
pH = ($IR_{IIa'}$ + 0.80)/0.20 (*n* = 26, R^2 = 0.83, RMSE 0.43)	Yang et al., 2015
MAAT = −8.57 + 31.45 × MBT'_{5ME} (*n* = 222, R^2 = 0.66, RMSE 4.8 °C)	De Jonge et al., 2014
MAATmr = 7.17 + 17.1 × (Ia) + 25.9 × (Ib) + 34.4 × (Ic) - 28.6 × (IIa) (n = 222, R^2 = 0.68, RMSE 4.6 °C)	De Jonge et al., 2014
MAAT = 31.21 × Index 1–7.98 (*n* = 20, R^2 = 0.77, RMSE 2.5 °C)	Wang et al., 2016
MAAT = 5.05 + 14.86 × Index 1 (n = 222, R^2 = 0.66, RMSE 4.8 °C)	De Jonge et al., 2014
MAATsr = 25.2–39.8 × f(IIIa)-29.8 × f(IIIa')-66.8 × f(IIa)-15.5 × f(IIa')-107.8 × f(IIb) + 25.1 × f(Ib) (*n* = 149, R^2 = 0.77, RMSE 2.5 °C)	Wang et al., 2020
MAAT = −20.14 + 39.61 × $MBT_{5/6}$ (*n* = 27, R^2 = 0.82, RMSE 1.3 °C)	Ding et al., 2015
MAAT = −10.82 + 28.36 × MBT'_{5ME} (n = 27, R^2 = 0.65, RMSE 1.8 °C)	Ding et al., 2015
MAAT = −8.57 + 31.45 × MBT'_{5ME} (n = 222, R^2 = 0.66, RMSE 4.8 °C)	De Jonge et al., 2014
MASTsr = 26.1–13.8 × f(IIIa)-27.9 × f(IIIa')-69.3 × f(IIa)-10 × f (IIa')-73.8 × f(IIb)-22.3 × f(IIb') + 21.7 × f(Ib) (n = 20, R^2 = 0.77, RMSE 2.5 °C)	Wang et al., 2020

3. Results and discussion

3.1. Extreme drought events during glacial periods on the NETP

In this paper, we identify extreme drought events based on $R_{i/b}$ values greater than 0.5, as reported in previous studies (e.g., Xie et al., 2013; Tang et al., 2017a). We also reconstruct hydrological variations using GDGT-0/Cren and $IR_{IIa'}$, with higher values indicating arid climate conditions (Yang et al., 2015; Qian et al., 2019; Lu et al., 2021).

The extreme drought events and hydrological variations exhibit three notable features. First, the NETP experienced significant drying during glacial periods. As shown in Fig. 2B, $R_{i/b}$ values of the Menyuan loess section remained consistently low and stable throughout interglacial periods. However, $R_{i/b}$ values exhibit a marked increase in both magnitude and frequency during glacial periods, particularly in MIS 2–4, followed by MIS 8 and MIS 6 (Fig. 2B). This is also supported by GDGT-0/Cren (Fig. 2C) and grain size (Fig. 2F) records. The minimal difference in soil pH (Fig. 2D) between glacial and interglacial periods may be due to influences other than climate, such as soil organic matter and structure (Six et al., 2004; Kaiser and Kalbitz, 2012). $R_{i/b}$, grain size, and GDGT-0/Cren records did not always correspond in detail (e.g., during MIS 2), which may be due to the indicators having multiple significances. Specifically, hydrological variations inferred from GDGTs (GDGT-0/Cren and $R_{i/b}$) may be biased toward local summer climate conditions, as GDGT-producing bacteria tend to thrive in the warm season (Gao et al., 2012; Peterse et al., 2014; Lu et al., 2019). In contrast,

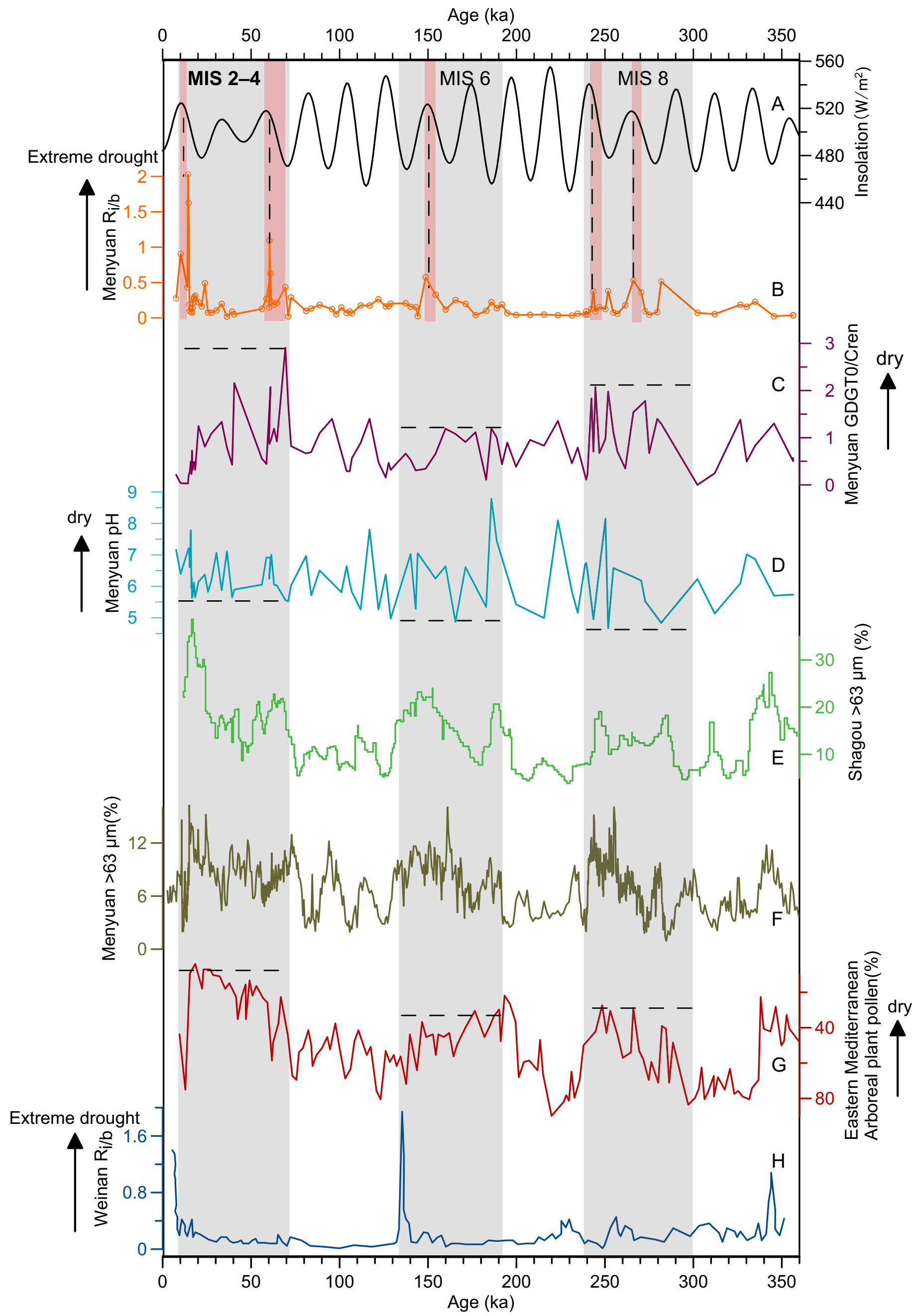

Fig. 2. Paleo-humidity variations of the NETP and compared with other records. (A) 37°N summer insolation (Berger and Loutre, 1991); (B) $R_{i/b}$, (C) GDGT-0/Cren and (D) pH records from the Menyuan loess section (This study). Dashed lines indicate minimum values during glacial periods; (E) Proportion of >63 μm particle size from the Shagou loess section (Wu et al., 2001); (F) Proportion of >63 μm particle size from the Menyuan loess section (Tian et al., 2022); (G) Proportion of arboreal plant pollen from the eastern Mediterranean (Gasse et al., 2015); (H) $R_{i/b}$ record from the Weinan loess section (Tang et al., 2017a). Gray shadings represent glacial periods.

grain size record mainly reflects climate signals from winter, as loess is mainly deposited during the winter due to strong winds. Additionally, differences between the values of GDGT-0/Cren and $R_{i/b}$ may arise from the use of different formulas. In general, despite these detailed differences, the climate variations indicated by these proxies generally align on an orbital scale.

A second feature is that the driest interval during glacial periods of the NETP over the last 350 ka occurred during the last glacial periods. $R_{i/b}$ and GDGT-0/Cren values were highest during this period, followed by MIS 8, with no remarkable changes observed during MIS 6 (Fig. 2B and C). Additional evidence for the extreme drought conditions during the last glacial period is provided by soil pH. Minimum pH values in the last glaciation were higher than those in other glacial periods, although differences between glacial and interglacial periods are not pronounced (Fig. 2D). This phenomenon has also been observed around the NETP. The proportion of particles larger than 63 μm at the Shagou (Fig. 2E; Wu et al., 2001) and Wuwei loess (Wu et al., 2002) sections near the Qilian mountains increased during the last glaciation compared to previous levels, reaching its maximum over the last 350 ka, indicating an extremely arid climate and intensified desertification during that period. This is further supported by the $\delta^{13}C$ record from the Ganzi loess section, and grain size as well as Na/K records from the Luhuo loess section on the eastern Tibetan Plateau (Qiao et al., 2014). In contrast, the driest period over the last 350 ka at the Weinan section (see Fig. 1A for the location) on the East Chinese Loess Plateau occurred during MIS 6, as evidenced by a remarkable rise in $R_{i/b}$ values (Fig. 2H; Tang et al., 2017a), rather than during the last glaciation. This is corroborated by grain size records from the Mangshan (Zheng et al., 2007) and Fanshan (Xiong et al., 2001) loess sections on the Chinese Loess Plateau. Therefore, the enhanced drought during glacial periods on the NETP was different from that on the East Chinese Loess Plateau. Notably, GDGT-derived peak aridity events in the NETP (Fig. 2B) correlate with boreal summer insolation maxima (Fig. 2A; Berger and Loutre, 1991) during glacial periods. This phenomenon has not been observed at the Weinan loess section (Tang et al., 2017a).

3.2. Mechanisms for the extreme drought on the NETP

Compared to the grain size data (Fig. 2F; Tian et al., 2022; Xiao et al., 2023), the new GDGTs data (Figs. 2B–D) reveal several novel features that differ from those observed in the Weinan loess section on the East Chinese Loess Plateau, as discussed in Section 3.1. These differences are attributed to the greater sensitivity of GDGT records to 'extreme drought' during the warm season compared to grain size. In this section, we further explore the mechanisms behind the extreme drought on the NETP.

The GDGT records indicate that extreme droughts on the NETP occurred during glacial periods rather than interglacial periods, suggesting that glacial conditions primarily control drought in the region. A colder glacial climate generally leads to drier conditions. Furthermore, peak aridity events (Fig. 2B) on the NETP show a strong correlation with boreal summer insolation maxima (Fig. 2A) during glacial periods, which can be explained by the direct influence of insolation via modulating evaporation. Soil-climate coupled simulations have shown that both precipitation and evaporation are important factors for paleosol development in North China (Finke et al., 2017; Ranathunga et al., 2023). Additionally, effective moisture, rather than temperature or precipitation alone, is suggested to play a crucial role in controlling soil development on the NETP (Liu et al., 2022). Consequently, increased insolation during glacial periods would enhance soil evaporation, leading to a reduction in soil water content and a corresponding increase in $R_{i/b}$ values.

The extent of drought on the NETP varies between glacial periods, with the driest interval occurring during the last glacial period. Moreover, significant differences in extreme drought between the NETP and the East Chinese Loess Plateau (e.g., Zheng et al., 2007; Tang et al., 2017a) cannot be fully explained by the direct impact of insolation alone. Our previous study indicates that the EASM weakened after MIS 8 due to paleo-ENSO (Tian et al., 2022). Therefore, we propose that during glacial periods, the influence of the Westerlies surpassed that of the EASM and became the primary driver of intensified drought on the NETP. This hypothesis is supported by several lines of evidence. Firstly, the arid climate during glacial periods on the NETP closely resembles that of Westerlies-dominated regions (Ayalon et al., 2002; Gasse et al., 2015), rather than regions influenced by the East Asian monsoon. For instance, the pollen-inferred vegetation from the Yammouneh basin in the eastern Mediterranean exhibited a significant decrease during the last glacial period (Fig. 2G), suggesting that last glaciation was relatively dry compared to other glacial periods over the last 430 ka (Gasse et al., 2015). Secondly, a gradual reduction in C_4 plants in the Tajikistan loess section, resulting from increased summer precipitation, indicates a southward shift of the Westerlies since MIS 8 (Yang and Ding, 2006). Thirdly, detrital zircon ages from the Menyuan loess indicate that the Qaidam and Tarim basins to the west were significant source areas for loess deposition on the NETP during glacial periods (Xiao et al., 2023). This finding supports the notion that prevailing Westerlies dominated the NETP during glacial periods, as also suggested by other studies (Tian et al., 2020; Kapp et al., 2011). However, the climate over the East Chinese Loess Plateau during glacial periods was mainly influenced by the East Asian monsoon (Tang et al., 2017a). Consequently, extreme drought events on the NETP over the past 350 ka may be linked to both variations in insolation and changes in the Westerlies. We do not discount the influence of the winter monsoon on the NETP. Grain size variations in the Menyuan loess exhibit a 100 kyr periodicity, consistent with records from the eastern and central Chinese Loess Plateau (Hao et al., 2012), indicating the presence of winter monsoon effects in this region. Here, we emphasized the impact of the Westerlies, primarily because the arid events inferred from GDGTs reflect climate changes in warm seasons rather than in winter.

3.3. Paleo-temperature variations on the NETP

We reconstructed the paleo-temperature variations (Fig. 3) over the last 350 ka using various brGDGT-derived proxies and their calibrations. Figs. 3A–C show the paleo-temperature changes produced from the MAATmr and Index 1 proxies. However, glacial-interglacial cycles are not discernible from these two proxies. In contrast, paleo-temperature curves (Figs. 3D–G) estimated by MAATsr, $MBT_{5/6}$, and MBT'_{5ME}—calibrated against MAAT on both global and regional scales (e.g., Tibetan Plateau, North China)—exhibit the same trends, with higher temperatures during interglacial periods and lower temperatures during glacial periods, although the amplitudes of temperature changes differ. This suggests that MBT'_{5ME}, $MBT_{5/6}$, and MAATsr might be more applicable for reconstructing paleo-temperature in the Menyuan region. It is worth noting that the temperature variations (Figs. 3D–G) inferred from these proxies exhibit a rather surprising feature: there was an unusual warming during the last glaciation, with temperatures even exceeding those estimated for the interglacial periods. This phenomenon has also been observed in other loess sections on the Chinese Loess Plateau; for example, calibrations from MBT'_{5ME} and Index1 for Weinan (Tang et al., 2017b) and Yuanbao (Guo et al., 2024) produce warmer temperatures during the last glaciation than during the Holocene. Global calibrations may show a less accurate MAAT than the regional calibrations (Yang et al., 2014; Wang et al., 2016), but this cannot explain the abnormal phenomena in this study, as both region (Figs. 3B, D, E, F, brown lines) and globe (Figs. 3A, C, G, green lines) calibrations show warming during the last glacial period.

Notably, GDGT-derived temperatures may reflect land surface temperatures rather than air temperatures (Wang et al., 2016, 2020; Lu et al., 2019), as GDGT producers thrive in the soil. In arid regions (Guo et al., 2024) and sparsely vegetated areas, soil temperatures can be higher than air temperatures (Wang et al., 2016, 2020; Lu et al., 2019). However, brGDGT temperature proxies and transfer functions (e.g., MBT'_{5ME}, Index1, $MBT_{5/6}$) have been developed based on air rather than soil temperature, which may introduce larger uncertainties in temperatures reconstruction. Wang et al. (2020) investigated the relationship between brGDGTs and soil temperature across a wide climatic gradient in China and developed a brGDGT-based mean annual soil temperature (MASTsr) index. Therefore, we further reconstructed the Menyuan land surface temperature changes using this proxy.

The temperature estimates derived from the MASTsr proxy for the last glacial period were lower than those for interglacial periods (Fig. 3H). This suggest that the MASTsr proxy, calibrated against soil temperatures, is more suitable for temperature reconstruction compared to other proxies calibrated against air temperatures (e.g., MBT_{5ME}、$MBT_{5/6}$、Index1). However, the temperature estimate for the last glaciation was still higher than for other glacial periods (Fig. 3H), indicating that unusual warming did occur during that time.

The MASTsr calibration yielded land surface temperatures ranging from −5 °C to 15 °C (Fig. 3H). During glacial periods, the average temperature in Menyuan was around 2.6 °C, with 4.8 °C in MIS 2–4, 4.6 °C in MIS 6, and − 1.5 °C in MIS 8 (Fig. 3H). Conversely, the average temperature was around 6.7 °C during interglacial periods, with 5.1 °C in MIS 5, 7.5 °C in MIS 7, and 7.7 °C in MIS 9 (Fig. 3H). Temperature peaks exceeding 12 °C (the modern warm season temperature of Menyuan) occurred at approximately 15 ka, 30 ka, 70 ka, 100 ka, 130

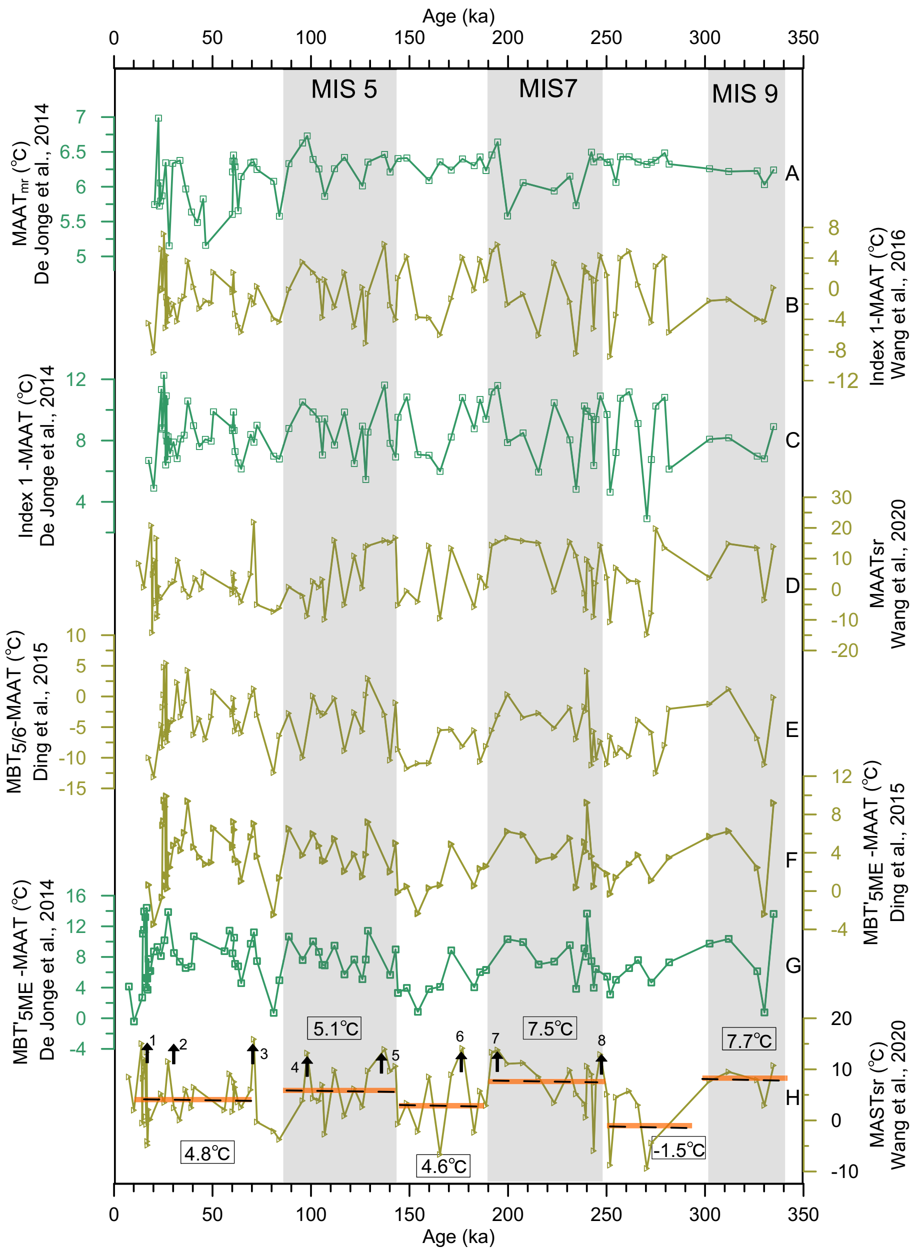

Fig. 3. The Menyuan temperature variations reconstructed from the various brGDGT-based proxies and calibrations. Gray shadings represent interglacial periods. The values inside the boxes represent the average temperatures during glacial and interglacial periods. Numbers 1–8 represent the temperature peaks exceeding 12 °C (the modern warm season temperature of Menyuan). Dashed lines represent average temperature values during glacial or interglacial periods. MBT′: Methylation index of Branched Tetraethers. MBT'_{5ME}: Exclusion of the 6-methyl brGDGTs from the MBT′. MAAT: Mean Annual Air Temperature. MAST: Mean Annual Soil Temperature.

ka, 175 ka, 195 ka, and 245 ka (Fig. 3H). The land surface temperature difference between glacial and interglacial periods is approximately 4.1 °C, which is consistent with the pollen record from this region (Herzschuh et al., 2006). Furthermore, GDGT-derived minimum and maximum temperatures exhibit an increasing trend from northwest China (Figs. 4G and H; Lu et al., 2019) to southeast China (Fig. 4I; Tang et al., 2017b), aligning with the modern temperature pattern.

3.4. Mechanisms for the paleo-temperature variations on the NETP

Temperature peaks of the NETP at approximately 245 ka, 195 ka, 175 ka, 130 ka, and 100 ka before the last glacial period align with local summer insolation maxima at 37°N (Fig. 4), suggesting that insolation is one of the factors contributing to the temperature variations on the NETP. In addition to insolation, changes in CO_2 levels could also contribute to these temperature variations. For instance, there is a clear decoupling between temperature and insolation at ~ 220 ka and ~ 200 ka (Figs. 4B and C). Land surface temperatures in Menyuan were ~ 5 °C and ~ 13 °C at ~ 220 ka and ~ 200 ka (Fig. 4C), respectively, while insolation was higher at 220 ka compared to 200 ka (Fig. 4B). Notably, CO_2 levels increased by 50 ppmv, from 200 ppmv at ~ 220 ka to 250 ppmv at ~ 200 ka (Fig. 4A; Lüthi et al., 2008). The higher temperature at 200 ka compared to 220 ka is consistent with the increase in CO_2 levels, suggesting that the cooling tendency induced by decreased insolation could be counteracted by the warming effect of increased CO_2. Consequently, temperature variations over the NETP may be influenced by both changes in insolation and CO_2 levels.

However, there are some temperature peaks (Fig. 4C) before the last

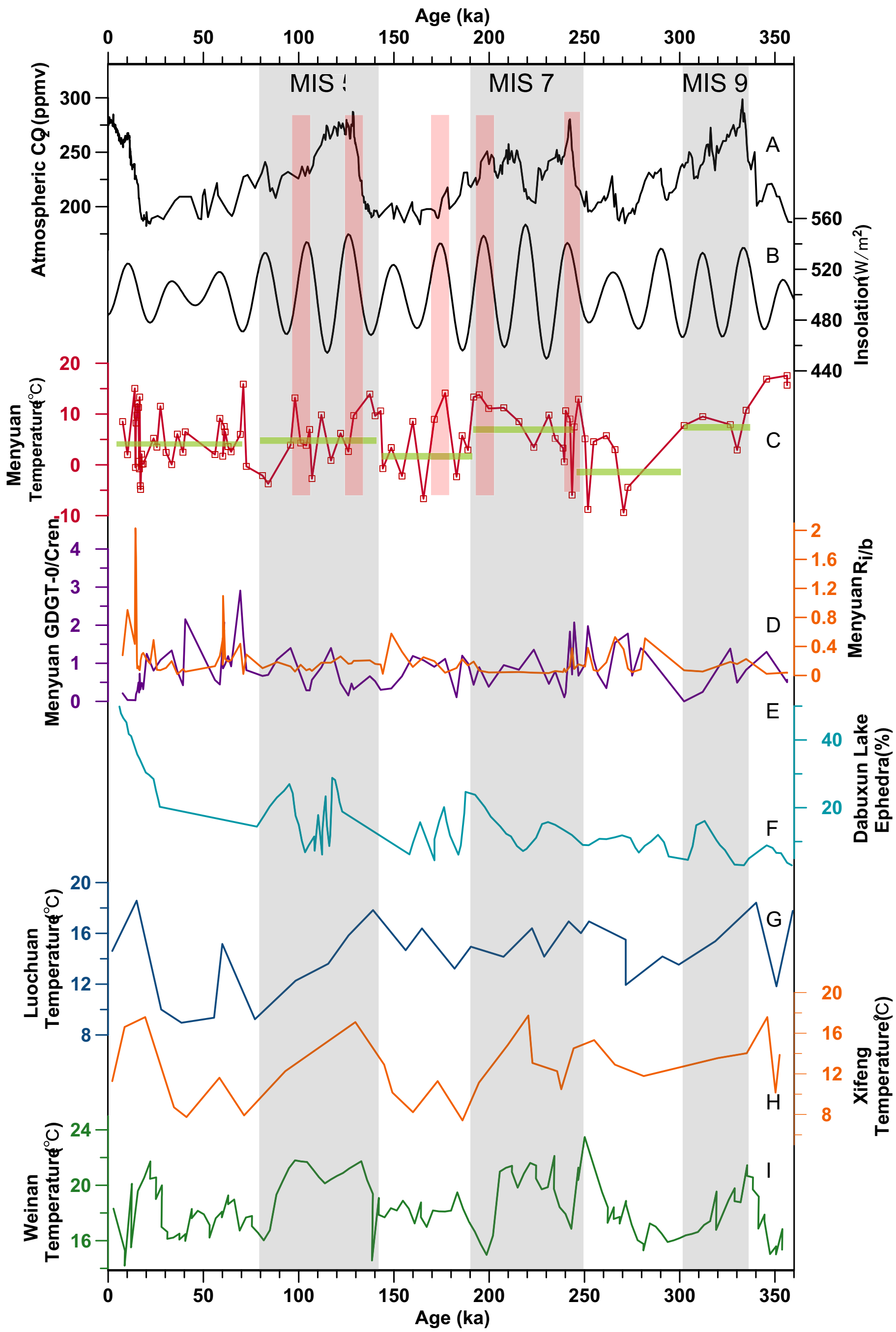

Fig. 4. Paleo-temperature record from the Menyuan loess section and compared with other records. (A) Atmospheric CO_2 concentration from Antarctic ice cores (Lüthi et al., 2008); (B) Summer insolation at 37°N (Berger and Loutre, 1991); (C) Paleo-temperature record based on the GDGTs from the Menyuan loess section (This study); (D) GDGT-0/Cren and (E) $R_{i/b}$ record from the Menyuan loess section (This study); (F) Ephedra record from Dabuxun Lake on the NETP (Jiang and Yang, 2001); Paleo-temperature records based on GDGTs from (G) Luochuan (Lu et al., 2019), (H) Xifeng (Lu et al., 2019), and (I) Weinan (Tang et al., 2017b) loess sections. Gray shadings represent interglacial periods.

glacial period that do not correspond to insolation maxima (Fig. 4A) or high CO_2 values (Fig. 4B), such as that around 160 ka. The Tibetan Plateau, which has the largest cryospheric extent outside the polar regions, may have its temperature variations influenced by its unique environmental conditions and internal climate feedback mechanisms, such as ice-albedo feedback. Glacial retreats in the Tibetan Plateau during MIS 6 (Owen and Dortch, 2014) would have reduced the reflection of solar radiation due to glacier shrinkage, potentially leading to a temperature rise around 160 ka. Further research is required to confirm this.

The unusual warming during the last glacial period cannot be explained by changes in insolation or CO_2, as neither showed significant variations compared to other glacial periods. Notably, besides unusual warming, the last glacial period was also the driest interval spanning the last 350 ka. Menyuan $R_{i/b}$ and the soils pH values reached their maxima during this period (Figs. 2B–D), indicating a remarkable decrease in soil moisture. Compared the relatively wet soil of other glacial periods, the dry soil during the last glacial period had a lower heat capacity and could absorb more heat from solar radiation, leading to higher land surface temperatures (Guo et al., 2024).

Simultaneously, vegetation may also have played an important role in the land surface temperature inferred from the GDGTs (Wang et al., 2016, 2020; Lu et al., 2019; Liang et al., 2019). A significant reduction in vegetation would decrease plant canopy and litter, further reduce the reflection of solar radiation and increase the radiation absorption by the soils (Ni et al., 2019). We suspect that the significant drying during the last glacial period could have led to a substantial decline in vegetation, as humidity is a crucial limiting factor for vegetation in the NETP (Herzschuh et al., 2006). The proportion of *Chenopodiaceae* and *Ephedra*, taxa traditionally used to represent deserts, from the Dabuxun Lake was notably increased during the last glacial period compared to prior levels and reached its maximum over the last 500 ka (Fig. 4F; Jiang and Yang, 2001), indicating vegetation degradation at that time. Further, Wu et al. (2001) indicate that the desert areas in the NETP reached their maximum extent during the last glacial period, spanning the last 900 ka (Fig. 2E). Numerous studies also demonstrate that a desert steppe or desert developed in the region (e.g., Shen et al., 2005; Herzschuh et al., 2006, 2009; Jin et al., 2015; Li et al., 2017). A significant reduction in vegetation would contribute to the unusual warming of land surface temperatures. Consequently, we propose that the unusual warming of land surface temperature during the last glacial period may be related to soil moisture and vegetation, with both factors potentially being equally important.

4. Conclusions

This research investigates variations in paleo-hydrology and paleo-temperature, as well as their underlying mechanisms over the north-eastern Tibetan Plateau (NETP), using Glycerol Dialkyl Glycerol Tetraethers (GDGTs) spanning the last 350 ka. The findings reveal that the NETP experienced significant drying during glacial periods, with the driest interval in the region occurring during the last glacial period. This contrasts with the monsoonal Chinese Loess Plateau. The extreme drought during glacial periods appears to be primarily controlled by local insolation and the Westerlies, due to the attenuation of East Asian summer monsoon (EASM). Our study underscores the sensitivity of climate variations over the NETP to insolation and Westerlies due to its high altitude. The reconstructed land surface temperature variations exhibit significant glacial-interglacial cycles, with temperatures during interglacial periods being approximately 4.1 °C higher than during glacial periods. Temperature changes in the region may be induced by changes in insolation, CO_2 levels, and internal climate feedback. The unusual warming during the last glaciation may be induced by soil moisture and vegetation related to drought. Our study provides the first long-scale paleo-temperature record for the NETP, highlight the pivotal roles of soil moisture and vegetation in land surface temperature variations.

Supplementary data to this article can be found online at https://doi.org/10.1016/j.palaeo.2024.112507.

CRediT authorship contribution statement

Shaohua Tian: Writing – review & editing, Writing – original draft, Visualization, Methodology, Investigation, Data curation. **Gaowen Dai:** Methodology, Investigation, Data curation. **Guoqiao Xiao:** Writing – review & editing, Supervision, Resources, Funding acquisition, Conceptualization. **Huan Yang:** Writing – review & editing, Software, Methodology, Data curation. **Xiaoqing Meng:** Investigation, Data curation. **Qiuzhen Yin:** Writing – review & editing.

Declaration of competing interest

The authors declare that they have no known competing financial interests or personal relationships that could have appeared to influence the work reported in this paper.

Data availability

Supplementary data to this article can be found online

Acknowledgments

This study is supported by the National Science Foundation of China (Grant nos. 42488201, 42272217) and the “Strategic Priority Research Program” of the Chinese Academy of Sciences (Grants: XDB26000000). Q.Z. Yin is Research Associate of the Fonds de la Recherche Scientifique FNRS (F.R.S.-FNRS).

References

An, Z.S., Colman, S.M., Zhou, W.J., Li, X.Q., Eric, T.B., Timothy, J.A.J., Cai, Y.J., Huang, Y.S., Lu, X.F., Chang, H., Song, Y.G., Sun, Y.B., Xu, H., Liu, W.G., Jin, Z.D., Liu, X.D., Cheng, P., Liu, Y., Ai, L., Li, X.Z., Liu, X., Yan, L., Shi, Z.G., Wang, X.L., Wu, F., Qiang, X.K., Dong, J.B., Lu, F.Y., Xu, X.W., 2012. Interplay between the Westerlies and Asian monsoon recorded in Lake Qinghai sediments since 32 ka. Sci. Rep. 2, 619. https://doi.org/10.1038/srep00619.

Ayalon, A., Bar-Matthews, M., Kaufman, A., 2002. Climatic conditions during marine oxygen isotope stage 6 in the eastern Mediterranean region from the isotopic composition of speleothems of Soreq Cave, Israel. Geology 30, 303–306. https://doi.org/10.1130/0091-7613(2002)030<0303:CCDMOI>2.0.CO;2.

Berger, A., Loutre, M.F., 1991. Insolation values for the climate of the last 10 million years. Quat. Sci. Rev. 10, 297–317. https://doi.org/10.1016/0277-3791(91)90033-Q.

Chen, D.L., Xu, B.Q., Yao, T.D., 2015. Assessment of past, present and future environmental changes on the Tibetan Plateau. Chin. Sci. Bull. 1–11. https://doi.org/10.1360/N972014-01370.

Chen, F.H., Wu, D., Chen, J.H., Zhou, A.F., Yu, J.Q., Shen, J., Wang, S.M., Huang, X., 2016. Holocene moisture and East Asian summer monsoon evolution in the northeastern Tibetan Plateau recorded by Lake Qinghai and its environs: a review of conflicting proxies. Quat. Sci. Rev. 154, 111–129. https://doi.org/10.1016/j.quascirev.2016.10.021.

Cheng, B., Chen, F.H., Zhang, J.W., 2013. Palaeovegetational and palaeoenvironmental changes since the last deglacial in Gonghe Basin, northeast Tibetan Plateau. J. Geogr. Sci. 23, 136–146. https://doi.org/10.1007/s11442-013-0999-5.

Cheng, H., Edwards, R.L., Sinha, A., Spötl, C., Yi, L., Chen, S.T., Kelly, M., Kathayat, G., Wang, X.F., Li, X.L., Kong, X.G., Wang, Y.J., Ning, Y.F., Zhang, H.W., 2016. The Asian monsoon over the past 640,000 years and ice age terminations. Nature 534, 640–646. https://doi.org/10.1038/nature18591.

Dang, X.Y., Yang, H., Naafs, B.D.A., Pancost, R.D., Xie, S.C., 2016. Evidence of moisture control on the methylation of branched glycerol dialkyl glycerol tetraethers in semi-arid and arid soils. Geochim. Cosmochim. Acta 189, 24–36. https://doi.org/10.1016/j.gca.2016.06.004.

De Jonge, C., Hopmans, E.C., Zell, C.I., Kim, J.H., Schouten, S., Sinninghe Damsté, J.S., 2014. Occurrence and abundance of 6-methyl branched glycerol dialkyl glycerol tetraethers in soils: implications for palaeoclimate reconstruction. Geochim. Cosmochim. Acta 141, 97–112. https://doi.org/10.1016/j.gca.2014.06.013.

Ding, Y.H., Chan, J.C.L., 2005. The East Asian summer monsoon: an overview. Meteorog. Atmos. Phys. 89, 117–142. https://doi.org/10.1007/s00703-005-0125-z.

Ding, S., Xu, Y., Wang, Y., He, Y., Hou, J., Chen, L., He, J.S., 2015. Distribution of branched glycerol dialkyl glycerol tetraethers in surface soils of the Qinghai–Tibetan Plateau: implications of brGDGTs-based proxies in cold and dry regions. Biogeosciences 12, 3141–3151. https://doi.org/10.5194/bg-12-3141-2015.

Duan, Y.W., Sun, Q., Werne, J.P., Zhao, H., Zhang, D.J., Zhang, N.M., Wu, J.B., Liu, D., Chen, F.H., 2019. Mid-Holocene moisture maximum revealed by pH changes derived from branched tetraethers in loess deposits of the northeastern Tibetan Plateau. Palaeogeogr. Palaeoclimatol. Palaeoecol. 520, 138–149. https://doi.org/10.1016/j.palaeo.2019.01.034.

Fan, Q.S., Ma, H.Z., Wei, H.C., An, F.Y., 2014. Holocene Lake-level changes of Hurleg Lake on northeastern Qinghai-Tibetan Plateau and possible forcing mechanism. The Holocene 0, 1–10. https://doi.org/10.1177/0959683613517399.

Finke, P., Yin, Q.Z., Bernardini, N.J., Yu, Y.Y., 2017. Climate-soil model reveals causes of differences between Marine Isotope Stage 5e and 13 paleosols. Geology 46, 99–102. https://doi.org/10.1130/G39301.1.

Gao, L., Nie, J.S., Clemens, S., Liu, W.G., Sun, J.M., Zech, R., Huang, Y.S., 2012. The importance of solar insolation on the temperature variations for the past 110 kyr on the Chinese Loess Plateau. Palaeogeogr. Palaeoclimatol. Palaeoecol. 317–318, 128–133. https://doi.org/10.1016/j.palaeo.2011.12.021.

Gasse, F., Vidal, L., Campo, E.V., Demory, F., Develle, A.L., Tachikawa, K., Elias, A., Bard, E., Garcia, M., Sonzogni, C., Thouveny, N., 2015. Hydroclimatic changes in northern Levant over the past 400,000 years. Quat. Sci. Rev. 111, 1–8. https://doi.org/10.1016/j.quascirev.2014.12.019.

Guo, J., Ziegler, M., Wanders, N., Vreeken, M., Yin, Q., Lu, H., Fuchs, L., Dong, J., Sun, Y., Peterse, F., 2024. Robust land surface temperature record for North China over the past 21,000 years. Sci. Adv. 10, eadj4800. https://doi.org/10.1126/sciadv.adj4800.

Hao, Q., Wang, L., Oldfield, F., Peng, S., Qin, L., Song, Y., Xu, B., Qiao, Y., Bloemendal, J., Guo, Z., 2012. Delayed build-up of Arctic ice sheets during 400,000-year minima in insolation variability. Nature 490, 393–396. https://doi.org/10.1038/nature11493.

Herzschuh, U., Kürschner, H., Mischke, S., 2006. Temperature variability and vertical vegetation belt shifts during the last ~50,000 yr in the Qilian Mountains (NE margin of the Tibetan Plateau, China). Quat. Res. 66, 133–146. https://doi.org/10.1016/j.yqres.2006.03.001.

Herzschuh, U., Kramer, A., Mischke, S., 2009. Quantitative climate and vegetation trends since the late glacial on the northeastern Tibetan Plateau deduced from Koucha Lake pollen spectra. Quat. Res. 71, 162–171. https://doi.org/10.1016/j.yqres.2008.09.003.

Herzschuh, U., Birks, H.J.B., Mischke, S., Zhang, C., Böhner, J., 2010. A modern pollen–climate calibration set based on lake sediments from the Tibetan Plateau and its application to a late Quaternary pollen record from the Qilian Mountains. J. Biogeogr. 37, 752–766. https://doi.org/10.1111/j.1365-2699.2009.02245.x.

Hou, J., Huang, Y., Zhao, J., Liu, Z., Colman, S., An, Z., 2016. Large holocene summer temperature oscillations and impact on the peopling of the northeastern Tibetan Plateau. Geophys. Res. Lett. 43, 1323–1330. https://doi.org/10.1002/2015GL067317.

Hsu, H., Lin, S., 2007. Asymmetry of the tripole rainfall pattern during the East Asian summer. J. Clim. 20, 4443–4458. https://doi.org/10.1175/JCLI4246.1.

Jia, G.D., Rao, Z.G., Zhang, J., Li, Z.Y., Chen, F.H., 2013. Tetraether biomarker records from a loess-paleosol sequence in the western Chinese Loess Plateau. Front. Microbiol. 4. https://doi.org/10.3389/fmicb.2013.00199.

Jiang, D.X., Yang, H.Q., 2001. Palynological evidence for Climatic changes in Dabuxun Lake of Qinghai Province during the past 500000 years. Acta Sedimentol. Sin. 19, 101–106 (in Chinese with English Abstract). https://doi.org/10.3969/j.issn.1000-0550.2001.01.017.

Jin, Z.D., An, Z.S., Yu, J.M., 2015. Lake Qinghai sediment geochemistry linked to hydroclimate variability since the last glacial. Quat. Sci. Rev. 122, 63–73. https://doi.org/10.1016/j.quascirev.2015.05.015.

Kaiser, K., Kalbitz, K., 2012. Cycling downwards–dissolved organic matter in soils. Soil Biol. Biochem. 52, 29–32. https://doi.org/10.1016/j.soilbio.2012.03.017.

Kang, S.C., Xu, Y.W., You, Q.L., Flüge, W.A., Pepin, N., Yao, T.D., 2010. Review of climate and cryospheric change in the Tibetan Plateau. Environ. Res. Lett. 5, 015101. https://doi.org/10.1088/1748-9326/5/1/015101.

Kapp, P., Pelletier, J.D., Rohrmann, A., Heermance, R., Russell, J., Ding, L., 2011. Wind erosion in the Qaidam basin, Central Asia: implications for tectonics, paleoclimate, and the source of the Loess Plateau. GSA Today 21 (4/5), 4–10. https://doi.org/10.1130/GSATG99A.1.

Li, J.Y., Dodson, J., Yan, H., Cheng, B., Zhang, X.J., Xu, Q.H., Ni, J., Lu, F.Y., 2017. Quantitative precipitation estimates for the northeastern Qinghai-Tibetan Plateau over the last 18,000 years. J. Geophys. Res. Atmos. 122, 5132–5143. https://doi.org/10.1002/2016JD026333.

Li, Y., Peng, S.M., Liu, H.B., Zhang, X.Z., Ye, W.T., Han, Q., Zhang, Y.X., Xu, L.M., Li, Y. C., 2020. Westerly jet stream controlled climate change mode since the last glacial maximum in the northern Qinghai-Tibet plateau. Earth Planet. Sci. Lett. 549, 116529. https://doi.org/10.1016/j.epsl.2020.116529.

Liang, J., Russell, J.M., Xie, H.C., Lupien, R.L., Si, G.C., Wang, J., Hou, J.Z., Zhang, G.X., 2019. Vegetation effects on temperature calibrations of branched glycerol dialkyl glycerol tetraether (brGDGTs) in soils. Org. Geochem. 127, 1–11. https://doi.org/10.1016/j.orggeochem.2018.10.010.

Liu, Y., An, Z.S., Linderholm, H.W., Chen, D.L., Song, H.M., Cai, Q.F., Sun, J.Y., Tian, H., 2009. Annual temperatures during the last 2485 years in the mid-eastern Tibetan Plateau inferred from tree rings. Sci. China SerD-Earth Sci. 52, 348–359. https://doi.org/10.1007/s11430-009-0025-z.

Liu, X.J., Xiao, G.Q., Li, E.C.Y., Lai, X.Z., Yu, Z.P., L.P, Wang, Z., 2017. Accumulation and erosion of aeolian sediments in the northeastern Qinghai-Tibetan Plateau and implications for provenance to the Chinese Loess Plateau. J. Asian Earth Sci. 135, 166–174. https://doi.org/10.1016/j.jseaes.2016.12.034.

Liu, B., Zhao, H., Li, S.H., Jin, H.L., Li, Y., Wang, H.P., Sun, A.J., Xu, Y., Wang, K.Q., 2022. Asynchronous palaeosol development during the past 20 ka in response to climate change across the dune fields of the Asian summer monsoonal boundary, northern China. Earth Sci. Rev. 234, 104232. https://doi.org/10.1016/j.earscirev.2022.104232.

Lu, H.Y., Wang, X.Y., Ma, H.Z., Tan, H.B., Vandenberghe, J., Miao, X.D., Li, Z., Sun, Y.B., An, Z.S., Cao, G.C., 2004. The plateau monsoon variation during the past 130 kyr revealed by loess deposit at Northeast Qinghai-Tibet (China). Glob. Planet. Chang. 41, 207–214. https://doi.org/10.1016/j.gloplacha.2004.01.006.

Lu, H.Y., Vandenberghe, J., Miao, X.D., Tan, H.B., Ma, H.Z., 2006. Evidence for an abrupt climatic reversal during the last interglacial on the Northeast Qinghai-Tibetan Plateau. Quat. Int. 154–155, 136–140. https://doi.org/10.1016/j.quaint.2006.02.009.

Lu, H.Y., Wang, X.Y., Wang, X.D., 2012. Palaeoclimatic changes in northeastern Qinghai-Tibetan Plateau revealed by magnetostratigraphy and magnetic susceptibility analysis of thick loess deposits. Neth. J. Geosci. 91 (1/2), 189–198. https://doi.org/10.1017/S001677460000158X.

Lu, H.X., Liu, W.G., Wang, H.Y., Wang, Z., 2016. Variation in 6-methyl branched glycerol dialkyl glycerol tetraethers in Lantian loess–paleosol sequence and effect on paleotemperature reconstruction. Org. Geochem. 100, 10–17. https://doi.org/10.1016/j.orggeochem.2016.07.006.

Lu, H.X., Liu, W.G., Yang, H., Wang, H.Y., Liu, Z.H., Leng, Q., Sun, Y.B., Zhou, W.J., An, Z.S., 2019. 800-Kyr land temperature variations modulated by vegetation changes on Chinese Loess Plateau. Nat. Commun. 10, 1958. https://doi.org/10.1038/s41467-019-09978-1.

Lu, J., Yang, H., Griffiths, M.L., Burls, N.J., Xiao, G., Yang, J., Wang, J., Johnson, K.R., 2021. Asian monsoon evolution linked to Pacific temperature gradients since the late Miocene. Earth Planet. Sci. Lett. 563, 116882. https://doi.org/10.1016/j.epsl.2021.116882.

Lüthi, D., Floch, M.L., Bereiter, B., Blunier, T., Barnola, J.-M., Siegenthaler, U., Raynaud, D., Jouzel, J., Fischer, H., Kawamura, K., Stocker, T.F., 2008. High-resolution carbon dioxide concentration record 650,000–800,000 years before present. Nature 453, 379–382. https://doi.org/10.1038/nature06949.

Ma, Z.H., Feng, Z.T., Peng, T.J., Liu, S.P., Li, M., Guo, B.H., Li, X.M., Song, C.H., Zhao, Z. J., Li, J.J., 2020. Quaternary drainage evolution of the Datong River, Qilian Mountains, northeastern Tibetan Plateau, China. Geomorphology 353, 107021. https://doi.org/10.1016/j.geomorph.2019.107021.

Ni, J., Cheng, Y., Wang, Q., Ng, C.W.W., Garg, A., 2019. Effects of vegetation on soil temperature and water content: field monitoring and numerical modelling. J. Hydrol. 571, 494–502. https://doi.org/10.1016/j.jhydrol.2019.02.009.

Owen, L.A., Dortch, J.M., 2014. Nature and timing of Quaternary glaciation in the Himalayan–Tibetan orogen. Quat. Sci. Rev. 88, 14–54. https://doi.org/10.1016/j.quascirev.2013.11.016.

Peterse, F., Prins, M.A., Beets, C.J., Troelstra, S.R., Zheng, H.B., Gu, Z.Y., Schouten, S., Sinninghe Damsté, J.S., 2011. Decoupled warming and monsoon precipitation in East Asia over the last deglaciation. Earth Planet. Sci. Lett. 301, 256–264. https://doi.org/10.1016/j.epsl.2010.11.010.

Peterse, F., Meer, J., Schouten, S., Weijers, J.W.H., Fierer, N., Jackson, R.B., Kim, J.H., Sinninghe Damsté, J.S., 2012. Revised calibration of the MBT-CBT paleotemperature proxy based on branched tetraether membrane lipids in surface soils. Geochim. Mochim. Ac. 96, 215–229. https://doi.org/10.1016/j.gca.2012.08.011.

Peterse, F., Martínez-García, A., Zhou, B., Beets, C.J., Prins, M.A., Zheng, H., Eglinton, T. I., 2014. Molecular records of continental air temperature and monsoon precipitation variability in East Asia spanning the past 130,000 years. Quat. Sci. Rev. 83, 76–82. https://doi.org/10.1016/j.quascirev.2013.11.001.

Qian, S., Yang, H., Dong, C., Wang, Y., Wu, J., Pei, H., Xie, S.C., 2019. Rapid response of fossil tetraether lipids in lake sediments to seasonal environmental variables in a shallow lake in Central China: Implications for the use of tetraether-based proxies. Org. Geochem. 128, 108–121. https://doi.org/10.1016/j.orggeochem.2018.12.007.

Qiao, Y., Qi, L., Liu, Z., Wang, Y., Yao, H., Yang, J., Zhao, Z., 2014. Intensification of aridity in the eastern margin of the Tibetan Plateau since 300 ka BP inferred from loess-soil sequences, western Sichuan Province, Southwest China. Palaeogeogr. Palaeoclimatol. Palaeoecol. 414, 192–199. https://doi.org/10.1016/j.palaeo.2014.08.025.

Ranathunga, K.N., Finke, P.A., Yin, Q.Z., Wu, Z.P., Hao, Q.Z., Lu, H., 2023. Driving factors of interglacial paleosol formation on the Chinese loess plateau and the effect of precession and ice sheets. Quat. Sci. Rev. 300, 107911. https://doi.org/10.1016/j.quascirev.2022.107911.

Schouten, S., Hopmans, E.C., Sinninghe Damsté, J.S., 2013. The organic geochemistry of glycerol dialkyl glycerol tetraether lipids: a review. Org. Geochem. 54, 19–61. https://doi.org/10.1016/j.orggeochem.2012.09.006.

Shen, J., Liu, X.Q., Wang, S.M., Matsumoto, R., 2005. Palaeoclimatic changes in the Qinghai Lake area during the last 18,000 years. Quat. Int. 136, 131–140. https://doi.org/10.1016/j.quaint.2004.11.014.

Six, J., Bossuyt, H., Degryze, S., Denef, K., 2004. A history of research on the link between (micro) aggregates, soil biota, and soil organic matter dynamics. Soil Tillage Res. 79, 7–31. https://doi.org/10.1016/j.still.2004.03.008.

Stauch, G., Ijmker, J., Pötsch, S., Zhao, H., Hilgers, A., Diekmann, B., Dietze, E., Hartmann, K., Opitz, S., Wünnemann, B., Lehmkuhl, F., 2012. Aeolian sediments on the north-eastern Tibetan Plateau. Quat. Sci. Rev. 57, 71–84. https://doi.org/10.1016/j.quascirev.2012.10.001.

Sun, W., Zhao, S.J., Pei, H.Y., Yang, H., 2019. The coupled evolution of mid- to late Holocene temperature and moisture in the southeast Qaidam Basin. Chem. Geol. 528, 119–282. https://doi.org/10.1016/j.chemgeo.2019.119282.

Sun, Y.B., Clemens, S.C., Guo, F., Liu, X.X., Wang, Y., Yan, Y., Liang, L.J., 2021. High sedimentation-rate loess records: a new window into understanding orbital- and millennial-scale monsoon variability. Earth Sci. Rev. 220, 103731. https://doi.org/10.1016/j.earscirev.2021.103731.

Tang, C.Y., Yang, H., Pancost, R.D., Griffiths, M.L., Xiao, G.Q., Dang, X.Y., Xie, S.C., 2017a. Tropical and high latitude forcing of enhanced megadroughts in Northern China during the last four terminations. Earth Planet. Sci. Lett. 479, 98–107. https://doi.org/10.1016/j.epsl.2017.09.012.

Tang, C.Y., Yang, H., Dang, X.Y., Xie, S.C., 2017b. Comparison of paleo-temperature reconstructions using microbial tetraether thermometers of the Chinese loess-paleosol sequence for the past 350000 years. Sci. China SerD-Earth Sci 60, 1159–1170. https://doi.org/10.1007/s11430-016-9035-y.

Thomas, E.K., Huang, Y.S., Clemens, S.C., Colman, S.M., Morrill, C., Wegener, P., Zhao, J. T., 2016a. Changes in dominant moisture sources and the consequences for hydroclimate on the northeastern Tibetan Plateau during the past 32 kyr. Quat. Sci. Rev. 131, 157–167. https://doi.org/10.1016/j.quascirev.2015.11.003.

Thomas, E.K., Clemens, S.C., Sun, Y., Prell, W.L., Huang, Y., Gao, L., Liu, Z., 2016b. Heterodynes dominate precipitation isotopes in the East Asian monsoon region, reflecting interaction of multiple climate factors. Earth Planet. Sci. Lett. 455, 196–206. https://doi.org/10.1016/j.epsl.2016.09.044.

Tian, S.H., Xiao, G.Q., Dai, G.W., Lai, Z.P., 2020. Recovery of early Holocene paleowind direction from the Gonghe Basin in northeastern Tibetan Plateau and its implications for provenance of Chinese loess. Quat. Sci. 40, 95–104 (in Chinese with English abstract). 10.11928/j.issn.1001-7410.2020.01.09.

Tian, S.H., Dai, G.W., Yin, Q.Z., Meng, X.Q., Zhang, Z.S., Zhu, Z.M., Xiao, G.Q., 2022. Spatial differences in East Asian climate transition at ~260 ka and their links to ENSO. Quat. Sci. Rev. 296, 107805. https://doi.org/10.1016/j.quascirev.2022.107805.

Wang, H.Y., Liu, W.G., Lu, H.X., 2016. Appraisal of branched glycerol dialkyl glycerol tetraether-based indices for North China. Org. Geochem. 2016 (98), 118–130.

Wang, X.Y., Yi, S.W., Lu, H.Y., Vandenberghe, J., Han, Z.Y., 2017. Aeolian process and climatic changes in loess records from the northeastern Tibetan Plateau: Response to global temperature forcing since 30 ka. Paleoceanography 30, PA00271. https://doi.org/10.1002/2014PA002731.

Wang, H.Y., An, Z.S., Lu, H.X., Zhao, Z.H., Liu, W.G., 2020. Calibrating bacterial tetraether distributions towards in situ soil temperature and application to a loess-paleosol sequence. Quat. Sci. Rev. 231, 106172. https://doi.org/10.1016/j.quascirev.2020.106172.

Wang, M., Hou, J., Duan, Y., Chen, J., Li, X., He, Y., Li, S., Chen, F., 2021. Internal feedbacks forced Middle Holocene cooling on the Qinghai-Tibetan Plateau. Boreas 50, 1116–1130. https://doi.org/10.1111/bor.12531.

Weijers, J.W., Schouten, S., van den Donker, J.C., Hopmans, E.C., Sinninghe Damsté, J. S., 2007. Environmental controls on bacterial tetraether membrane lipid distribution in soils. Geochim. Cosmochim. Acta 71, 703–713. https://doi.org/10.1016/j.gca.2006.10.003.

Wischnewski, J., Mischke, S., Wang, Y.B., Herzschuh, U., 2011. Reconstructing climate variability on the northeastern Tibetan Plateau since the last Lateglacial-a multi-proxy, dual-site approach comparing terrestrial and aquatic signals. Quat. Sci. Rev. 30, 82–97. https://doi.org/10.1016/j.quascirev.2010.10.001.

Wu, T.W., Qian, Z.A., 2003. The relation between the Tibetan winter snow and the Asian summer monsoon and rainfall: an observational investigation. J. Clim. 16, 2038–2051. https://doi.org/10.1175/1520-0442(2003)016<2038:TRBTTW>2.0.CO;2.

Wu, G.J., Pan, B.T., Li, J.J., Guan, Q.Y., Liu, Z.G., 2001. Tectonic climate events in the eastern Qilian Mountains since 0.83 Ma. Sci. China Ser. D. 44, 251–260. https://doi.org/10.1360/yd2001-44-S1-251.

Wu, H.B., Guo, Z.T., Fang, X.M., Zhang, J., Chen, F.H., 2002. Extension of drylands in northern China around 250 ka BP linked with the uplift of the southeast margin of Tibetan Plateau. Chin. Sci. Bull. 47, 1739–1745. https://doi.org/10.1007/BF03183320.

Xiao, G.Q., Zong, K.Q., Li, G.J., Hu, Z.C., Dupont-Nivet, G., Peng, S.Z., Zhang, K.Q., 2012. Spatial and glacial-interglacial variations in provenance of the Chinese Loess Plateau. Geophys. Res. Lett. 39, L20715. https://doi.org/10.1029/2012GL053304.

Xiao, G.Q., Dai, G.W., Tian, S.H., Peng, S.Z., Li, L.T., Meng, X.Q., Yin, Q.Z., 2023. Periodic variations of alpine glaciation and desertification of the NE Tibetan Plateau: evidence from the loess-paleosol sequences in the Menyuan Basin. Glob. Planet. Chang. 226, 104160. https://doi.org/10.1016/j.gloplacha.2023.104160.

Xie, S.C., Richard, D.P., Chen, L., Evershed, R.P., Yang, H., Zhang, K.X., Huang, J.H., Xu, Y.D., 2013. Microbial lipid records of highly alkaline deposits and enhanced aridity associated with significant uplift of the Tibetan Plateau in the late Miocene. Geol. Soc. Am. 40. https://doi.org/10.1130/G32570.1, 291–241.

Xiong, S.F., Ding, Z.L., Liu, T.S., 2001. Climatic implications of loess deposits from the Beijing region. J. Quat. Sci. 16, 575–582. https://doi.org/10.1002/jqs.618.

Yang, S.L., Ding, Z.L., 2006. Winter-spring precipitation as the principal control on predominance of C_3 plants in Central Asia over the past 1.77 Myr: evidence from $\delta^{13}C$ of loess organic matter in Tajikistan. Palaeogeogr. Palaeoclimatol. Palaeoecol. 235, 330–339. https://doi.org/10.1016/j.palaeo.2005.11.007.

Yang, H., Pancost, R.D., Dang, X.Y., Zhou, X.Y., Evershed, R.P., Xiao, G.Q., Tang, C.Y., Gao, L., Guo, Z.T., Xie, S.C., 2014. Correlations between microbial tetraether lipids and environmental variables in Chinese soils: optimizing the paleo-reconstructions in semi-arid and arid regions. Geochim. Cosmochim. Acta 126, 49–69. https://doi.org/10.1016/j.gca.2013.10.041.

Yang, H., Lv, X.X., Ding, W.H., 2015. The 6-methyl branched tetraethers significantly affect the performance of the methylation index (MBT') in soils from an altitudinal transect at Mount Shennongjia. Org. Geochem. 82, 42–53. https://doi.org/10.1016/j.orggeochem.2015.02.003.

Yang, Y.B., Yang, R.S., Li, X.Y., Han, W.X., Zan, J.B., Fang, X.M., Appel, E., 2017. Glacial-interglacial climate change on the northeastern Tibetan Plateau over the last 600 kyr. Palaeogeogr. Palaeoclimatol. Palaeoecol. 476, 181–191. https://doi.org/10.1016/j.palaeo.2017.04.007.

Zeng, F.M., Yang, H., 2019. Temperature changes reconstructed from branched GDGTs on the central Loess Plateau during the past 130-5 ka. Quat. Int. 503, 3–9. https://doi.org/10.1016/j.quaint.2018.04.045.

Zhang, Y., Shao, X.M., Yin, Z.Y., Wang, Y., 2014. Millennial minimum temperature variations in the Qilian Mountains, China: evidence from tree rings. Clim. Past 10, 1763–1778. https://doi.org/10.5194/cp-10-1763-2014.

Zhao, H., Huang, C.C., Wang, H.Y., Liu, W., Qiang, X., Xu, X., Guo, Y., 2018. Mid-late Holocene temperature and precipitation variations in the Guanting Basin, upper reaches of the Yellow River. Quat. Int. 490, 74–81. https://doi.org/10.1016/j.quaint.2018.05.009.

Zhao, Y., Tzedakis, P.C., Li, Q., Qin, F., Cui, Q., Liang, C., Guo, Z., 2020. Evolution of vegetation and climate variability on the Tibetan Plateau over the past 1.74 million years. Sci. Adv. 6, eaay6193. https://doi.org/10.1126/sciadv.aay619.

Zheng, H., Huang, X., Ji, J., Liu, R., Zeng, Q., Jiang, F., 2007. Ultra-high rates of loess sedimentation at Zhengzhou since stage 7: implication for the Yellow River erosion of the sanmen gorge. Geomorphology 85, 131–142. https://doi.org/10.1016/j.geomorph.2006.03.014.

Zhu, H., Zheng, Y., Shao, X.M., Liu, X.H., Xu, Y., Liang, E.Y., 2008. Millennial temperature reconstruction based on tree-ring widths of Qilian juniper from Wulan, Qinghai Province, China. Sci. Bull. 53, 3914–3920. https://doi.org/10.1007/s11434-008-0400-8.

Zhu, Z., Wu, J., Chu, G., Rioual, P., Lu, J., Wang, L., Liu, J., 2024. Summer warming during Heinrich Stadial 1 in Northeast China. Geology 20, G51881. https://doi.org/10.1130/G51881.1.

Zou, F.L., Li, H.D., Hua, Q.W., 2020. Responses of vegetation greening and land surface temperature variations to global warming on the Qinghai-Tibetan Plateau, 2001-2016. Ecol. Indic. 119, 106867. https://doi.org/10.1016/j.ecolind.2020.106867.